Journal of Controlled Release 304 (2019) 102–110

Contents lists available at ScienceDirect

Journal of Controlled Release

journal homepage: www.elsevier.com/locate/jconrel

Characterizing the protein corona of sub-10 nm nanoparticles

Dylan Glancy[a,b], Yuwei Zhang[a,b,c], Jamie L.Y. Wu[b,c], Ben Ouyang[b,c], Seiichi Ohta[b,c,d], Warren C.W. Chan[a,b,c,e,f,*]

[a] Department of Chemistry, University of Toronto, 80 St. George Street, Toronto, ON M5S 3H6, Canada
[b] Terrence Donnelly Centre for Cellular and Biomolecular Research, University of Toronto, 160 College Street, Room 230, Toronto, ON M5S 3E1, Canada
[c] Institute of Biomaterials and Biomedical Engineering, University of Toronto, 164 College St, Toronto, ON M5S 3G9, Canada
[d] Center for Disease Biology and Integrative Medicine, The University of Tokyo, 7-3-1 Hongo Bunkyo-ku, Tokyo 113-8655, Japan
[e] Department of Chemical Engineering, University of Toronto, 200 College Street, Toronto, ON M5S 3E5, Canada
[f] Department of Material Science and Engineering, University of Toronto, 160 College Street, Room 450, Toronto M5S 3E1, Canada

ARTICLE INFO

Keywords:
Protein corona
Nanomedicine
Ultrasmall nanoparticles
Cargo
Carrier

ABSTRACT

Studies into the interactions of serum proteins with nanoparticles are typically performed using nanoparticles that are larger than the size of proteins. Due to this size discrepancy, adsorbed proteins are commonly depicted as a globular structure surrounding a nanoparticle. Here, we asked how we should view nanoparticle–protein complexes when the nanoparticles are of similar size or smaller than the proteins with which they interact. We showed that nanoparticles can serve as a cargo on a protein rather than as a carrier of the protein in a size-dependent manner. This can occur when nanoparticles are below 10 nm in diameter. We discovered that when the nanoparticle is a cargo on the protein, the binding of the protein to the receptor target is minimally affected in contrast to the nanoparticle serving as a carrier. Our study should change how we view and describe nanoparticle–protein complexes when the nanoparticles involved are equal in size or smaller than proteins.

1. Introduction

Nanoparticles can be engineered with precise sizes, shapes and surface chemistries in order to perform highly specialized therapeutic and diagnostic tasks in the body [1]. Upon their administration into the bloodstream, nanoparticles rapidly adsorb serum proteins [2]. This protein layer, termed the 'protein corona,' is hypothesized to direct downstream physiological responses, such as signalling [3], accumulation [4] and clearance [5], by imbuing nanoparticles with a new 'biological identity,' [6] which includes a surface chemistry, size and aggregation state distinct from the engineered specifications of the particle [7]. The composition [8], affinity [9], thickness [10] and other properties of the protein corona have been researched extensively for a variety of nanoparticle formulations. Most of these studies involve nanoparticles that are significantly larger than the size of serum proteins, and therefore the nanoparticles can be seen as the 'carrier' of protein 'cargo' (Fig. 1A). Researchers have generally assumed that this interpretation of the protein corona architecture and biological impact can be extrapolated to ultrasmall nanoparticles, which are typically particles that are smaller than 10 nm. Here, we find that below a diameter of 10 nm, nanoparticles incubated with human serum proteins begin to act as the cargo rather than the carrier in nanoparticle–protein complexes. We further show that complexes formed with ultrasmall nanoparticles retain the shape, size and function of the protein carrier (Fig. 1B). This new understanding of ultrasmall nanoparticle–protein interactions could lead to design strategies and utilities of nanoparticles in medical applications.

2. Results and discussion

2.1. Are sub-10 nm gold nanoparticles carriers or cargo?

We first evaluated the interactions of proteins with ultrasmall nanoparticles of a similar size to determine whether the nanoparticle could be considered a cargo. Here, we define a carrier as the component of the nanoparticle–protein complex that dominates the overall morphology of the complex (typically, the largest component in the complex) while a cargo is something that is being carried. Four-nanometer gold nanoparticles were synthesized by the reduction of chloroauric acid with a solution of tannic acid, sodium citrate and potassium carbonate. These 4 nm gold nanoparticles with citrate surface chemistry (4 nm–CIT) were used as a model nanoparticle, as they can be synthesized with a narrow size distribution (4.4 ± 0.4 nm, see Fig. SI-1) and their unpassivated (*i.e.* free of antifouling surface chemistries) surface

* Corresponding author at: Institute of Biomaterials and Biomedical Engineering, University of Toronto, 164 College St., Toronto, ON M5S 3G9, Canada
E-mail address: warren.chan@utoronto.ca (W.C.W. Chan).

https://doi.org/10.1016/j.jconrel.2019.04.023
Received 15 January 2019; Received in revised form 26 March 2019; Accepted 16 April 2019
Available online 17 April 2019

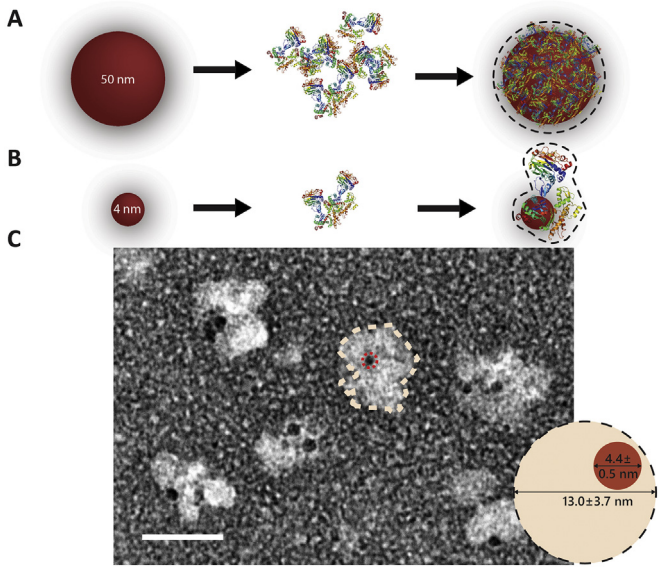

Fig. 1. A) and B) Schematic illustrations of nanoparticle incubations with human serum proteins. A) 50 nm nanoparticles incubated with proteins form complexes whose sizes and shapes are dictated by the nanoparticle. B) 4 nm nanoparticles incubated with proteins form a complex whose size and shape are dictated by the protein involved. The protein is considered a carrier and the nanoparticle is considered cargo. C) Negative-stain TEM imaging of 4 nm gold nanoparticles coated with citrate incubated with human serum with inlay showing a representation of average nanoparticle diameter and average complex diameter as quantified by image analysis. The image is annotated with an outline of a nanoparticle–protein complex in beige and a nanoparticle in red. $n = 416$ complexes, error bars represent the ± standard deviation of the radius. All scale bars represent 25 nm. (For interpretation of the references to colour in this figure legend, the reader is referred to the web version of this article.)

promoted rapid adsorption to serum proteins. We also chose 4 nm as a model nanoparticle diameter, as this size is comparable to that of proteins with molecular weights ranging from 20 to 100 kDa [11]. Nanoparticles were then incubated with human serum for one hour at 37 °C. It was necessary to use sucrose gradient purification to separate free proteins from the 4 nm–CIT particles based on density, as the high centrifugation speed required to sediment particles of this size also tended to sediment very large serum proteins. Following ultrafiltration through a 3 kDa membrane to remove sucrose, nanoparticles were negative-stained using a 1% uranyl acetate solution and observed by transmission electron microscopy (TEM). TEM images of negative-stained samples suggested that the shape of the complexes was dependent on protein shape rather than the shape of the particle (Fig. 1C). We also measured the size of nanoparticle–protein complexes from negative-stained TEM images and found that the size of the complexes was 3.0 ± 0.9 times larger than the diameter of the particles themselves (Fig. 1C inset). The size of particles relative to the protein led to large increases in the complex size. However, the stochastic interactions of ultrasmall nanoparticles with the diverse human serum proteins led to the formation of asymmetric and idiosyncratic complexes; therefore, the size of any individual complex is highly dependent on the proteins present. Dynamic light scattering (DLS) was not used because this technique is unable to detect ultrasmall nanoparticles due to their relatively small amount of light scattering in comparison to the scattering of aggregates or dust particles. The relative size increase of sub-10 nm nanoparticle–protein complexes that we observed in the present study illustrated the dramatic physical change that resulted from a small nanoparticle's adsorption as cargo to a protein carrier, a change that may affect subsequent physiological interactions of nanoparticles with cells and biological barriers.

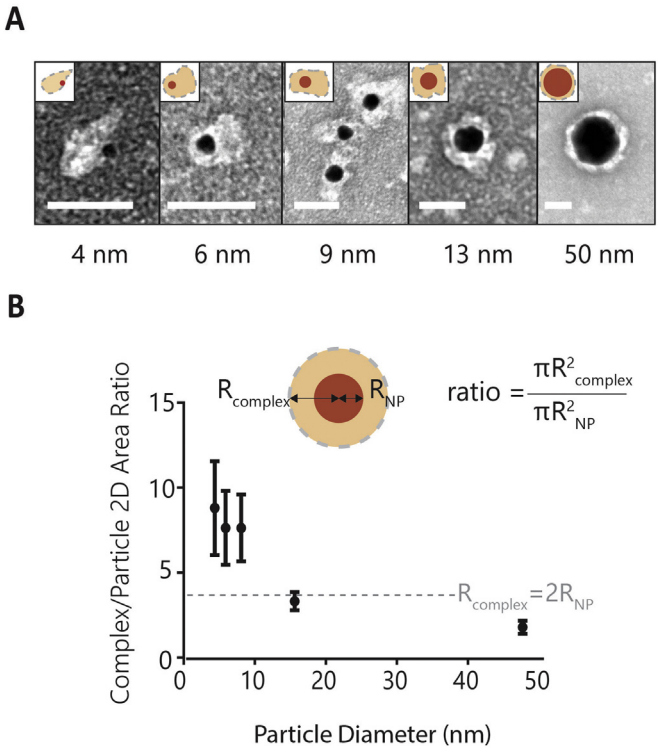

Fig. 2. A) Negative-stain TEM imaging of citrate-coated gold nanoparticles of various sizes incubated with human serum with inset illustration. All scale bars are 25 nm. (B) TEM images such as those in Fig. 2A were analyzed with image analysis software to determine the approximate area of the nanoparticle–protein complexes. Complex and particle two-dimensional area was extrapolated from imaged features' diameters and plotted against the gold nanoparticle diameter. Error bars represent the ± standard deviation of areas calculated from $n > 200$ complex and particle diameters. (For interpretation of the references to colour in this figure legend, the reader is referred to the web version of this article.)

2.2. Nanoparticle size determines whether ultrasmall nanoparticles are carriers

Having observed the cargo behaviour of 4 nm nanoparticles, we next questioned at what size a nanoparticle begins to act as a cargo rather than as a carrier of human serum proteins. Six-nanometer and 9 nm gold nanoparticles were synthesized by the reduction of chloroauric acid with tannic acid and sodium citrate (6 nm-CIT and 9 nm-CIT, respectively). Thirteen-nanometer gold nanoparticles were synthesized using the Turkevich method (13 nm-CIT), and 50 nm gold nanoparticles were synthesized using the Perrault method of seed growth due to the reduction of chloroauric acid with hydroquinone (50 nm-CIT) [12]. Normalizing to surface area, the 6 nm-CIT, 9 nm-CIT, 13 nm-CIT and 50 nm-CIT particles were incubated with human serum, washed and imaged with TEM. From negative-stained TEM images of the complexes at 10 proteins/nm^2, we observed that, whereas 50 nm-CIT and 13 nm-CIT nanoparticles formed a nanoparticle–protein complex with a size and shape determined by the nanoparticle, 4 nm-CIT, 6 nm-CIT and 9 nm-CIT nanoparticles clearly formed particle-on-protein complexes with the size and shape of the complex determined by the proteins present (Fig. 2A). To quantify these images, we measured the diameters (D) of the negative-stained complexes from our TEM images and calculated the area of the imaged complex; we did the same for the nanoparticles within the complexes. We then took a ratio of the two areas to determine how much larger the nanoparticle–protein complexes are compared to the nanoparticles (Eq. (1)).

$$ratio = \frac{\pi\left(\frac{D_{complex}}{2}\right)^2}{\pi\left(\frac{D_{nanoparticle}}{2}\right)^2} \quad (1)$$

We observed that the two-dimensional area of complexes increased 8.8 ± 2.7 times over the two-dimensional area of 4 nm-CIT particles, as opposed to only 3.3 ± 0.5 and 1.8 ± 0.4 times for 13 nm-CIT and 50 nm-CIT particles, respectively following incubation with 10 proteins/nm^2 (Fig. 2B). In absolute terms, the size increases were similar (see Fig. SI-2). However, this translated to a large difference relative to the size of the nanoparticles. Furthermore, we observed a transition between nanoparticle carrier and nanoparticle cargo complexes between nanoparticle diameters of 9 and 13 nm. It makes sense that the transition takes place between 9 and 13 nm if we assume that when the complex acquires an equivalent radius twice as large as the nanoparticle, the particle no longer dictates the overall size and morphology of the complex. By this classification, we can hypothesize that a threshold exists at a complex-to-nanoparticle two-dimensional area ratio of 4 (shown in grey dotted line in Fig. 2B). Drawing this line, we observe that it roughly separated the 4, 6 and 9 nm particles from the 13 and 50 nm particles. Additionally, sub-10 nm nanoparticles form complexes with a high degree of polydispersity when compared to the 13 and 50 nm nanoparticles. As cargo, the overall size of the nanoparticle–protein complexes formed with sub-10 nm nanoparticles are highly dependent on the adsorbed proteins. Human serum contains thousands of different proteins, and therefore the size of nanoparticle–protein complexes formed with sub-10 nm nanoparticles was highly variable, resulting in the large standard deviations represented by the error bars in Fig. 2B. In complexes formed with large nanoparticles, the nanoparticles play the role of the carrier. Therefore, variability in the size of the complexes is related to the variability in the size of nanoparticles. Since we can synthesize gold nanoparticles with very low polydispersity, the size of the complexes was relatively consistent, as can be seen in the small standard deviations observed for nanoparticle–protein complexes formed with 13 nm and 50 nm nanoparticles.

To further illustrate the transition of nanoparticles from carrier to cargo at nanoparticle diameters under 10 nm, we performed agarose gel electrophoresis on 4 nm-CIT, 6 nm-CIT, 9 nm-CIT, 13 nm-CIT and 50 nm-CIT particles incubated with bovine serum albumin (BSA) and compared them to the same batch of nanoparticles post-synthesis (Fig. 3A). We used a single protein, BSA, rather than whole human serum because it allowed us to isolate and visualize a single uniform band on the gel. We observed that the migration of the BSA-incubated sub-10 nm nanoparticles was retarded relative to 13 nm-CIT and 50 nm-CIT when compared to the non-incubated nanoparticles. This retardation is the result of a greater relative increase in nanoparticle–protein complex size for nanoparticles under 10 nm in diameter. Furthermore, when we quantified the migration distance of protein-incubated particles relative to that of a free nanoparticle of the same size (Eq. (2)), we saw that the protein has an effect on the migration distance of sub-10 nm nanoparticles (migrating only 20% to 23% of the migration distance of the free nanoparticle, Fig. 3B). This effect was less evident for the larger nanoparticles (32% for protein-incubated 13 nm-CIT particles and 46% for 50 nm-CIT particles). If we instead consider how the migration of BSA changes when incubated with nanoparticles by comparing the migration of incubated particles to the migration distance of the protein itself (Eq. (3), see Fig. SI-3), we see that the 4 nm-CIT nanoparticles migrated almost as far (71%) as the migration distance of the free protein, whereas the 50 nm-CIT nanoparticles migrated a short distance compared to the free protein (11%). We interpret this as the 50 nm-CIT nanoparticle playing a large role in determining the size, and therefore migration distance, of its nanoparticle–protein complex, whereas the smaller nanoparticles rely on the protein to dictate the size (and therefore migration) of their complexes, supporting our conclusion that for smaller nanoparticles, the nanoparticle's role in the complex changes from that of a carrier to that of cargo as a result of protein adsorption. Because sub-10 nm nanoparticles form complexes whose physical characteristics are dictated by those of the proteins, nanoparticle size becomes a less useful parameter in this range, and any sub-10 nm nanoparticle administered into the body will be recognized biologically as a complex with a size similar to that of the protein.

$$d_{relative \cdot NP} = \frac{migration_{NP+BSA}}{migration_{NP}} \quad (2)$$

$$d_{relative \cdot BSA} = \frac{migration_{NP+BSA}}{migration_{BSA}} \quad (3)$$

2.3. Surface chemistry of sub-10 nm nanoparticles impacts whether they can be deemed as a carrier or a cargo

After finding the point at which nanoparticles transition from carriers to cargo, we next investigated the effect of nanoparticle surface chemistry on whether the nanoparticle acts as a carrier or a cargo. Four-nanometer gold nanoparticles were functionalized with anionic surface chemistry 11-mercaptoundecanoic acid (4 nm-MUA), cationic surface chemistry 11-(mercaptoundecyl)-*N,N,N*-trimethylammonium bromide (4 nm-MUB) and neutral surface chemistry 1 kDa thiolated methoxy polyethylene glycol (4 nm-PEG). Successful conjugation of ligands was confirmed by agarose gel electrophoresis, DLS and zeta potential

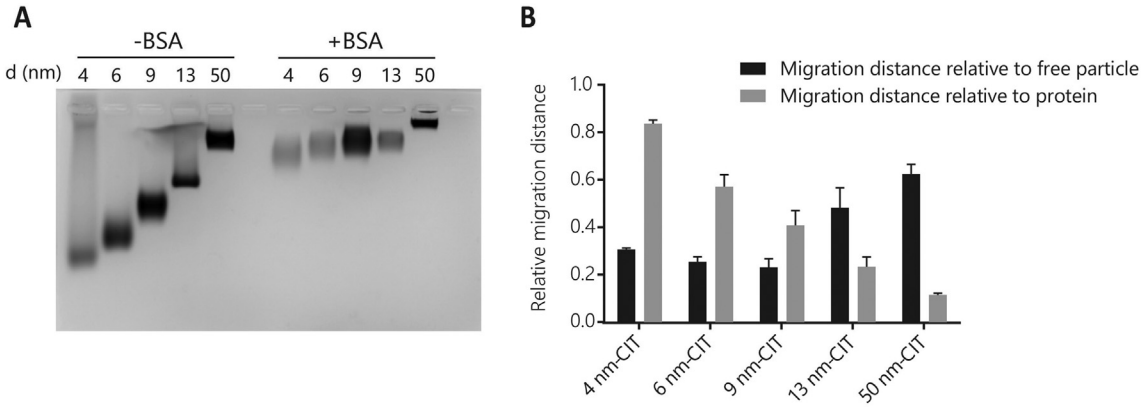

Fig. 3. A) Agarose gel electrophoresis of citrate-coated gold nanoparticles with or without incubation with BSA. B) The migration distance of citrate-coated nanoparticles incubated with BSA relative to free particles of the same size (black) and the migration distance of nanoparticles incubated with BSA relative to BSA protein stained with Krypton (grey). Error bars represent ± standard deviation of measurements of three incubation replicates on the same gel. (For interpretation of the references to colour in this figure legend, the reader is referred to the web version of this article.)

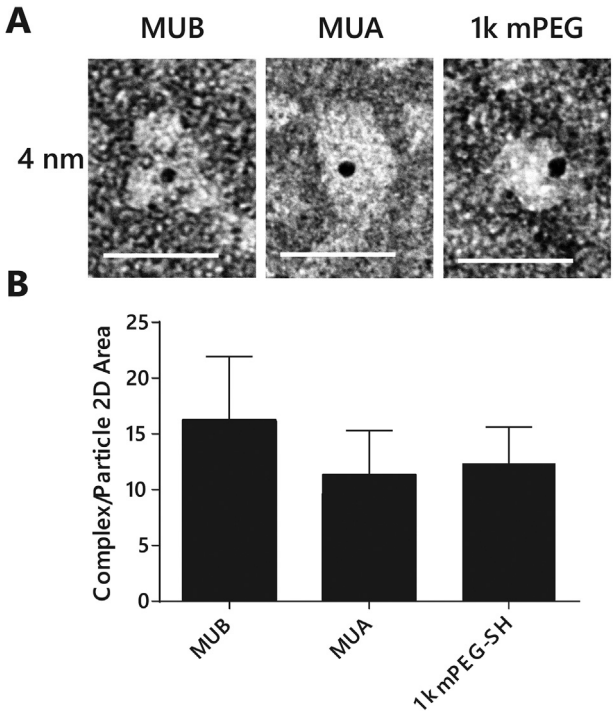

Fig. 4. A) Negative-stained TEM images of 4 nm gold nanoparticles with three different surface chemistries incubated with human serum at a ratio of 10 proteins/nm^2. The gold nanoparticles were coated with anionic surface chemistry 11-mercaptoundecanoic acid (4 nm-MUA), cationic surface chemistry 11-(mercaptoundecyl)-*N,N,N*-trimethylammonium bromide (4 nm-MUB), and neutral surface chemistry 1 kDa thiolated methoxy polyethylene glycol (4 nm-PEG). B) Image analysis of TEM images with areas calculated from the diameters of $n > 200$ complexes and particles. Error bars represent the standard deviation. Scale bars represent 25 nm. (For interpretation of the references to colour in this figure legend, the reader is referred to the web version of this article.)

measurements (see Fig. SI-1). Following incubation with human serum proteins and purification, we imaged the samples using TEM with a 1% solution of uranyl acetate negative stain, which colours inorganic areas dark thereby highlighting proteins. Our TEM results indicate that all of the surface chemistries tested formed nanoparticle–protein complexes that qualitatively have a shape and size determined by the proteins (Fig. 4A). Image analysis confirmed that the two-dimensional area of the nanoparticle–protein complex is > 10 times larger than the particle itself for all three surface chemistries, suggesting that regardless of surface chemistry, the complexes formed have nanoparticles as the cargo on the protein carrier (Fig. 4B). We then sought to determine whether the surface chemistry of the particle changed the size at which nanoparticles transition from cargo to carriers. We functionalized 6, 9, 13, and 50 nm gold nanoparticles with the ligands indicated above. We were surprised to see that 9 nm nanoparticles could be above or below the radius limit, suggesting that they may act as carriers or cargo depending on their surface chemistry (Fig. 5A). In contrast, 6 nm nanoparticles were cargo regardless of surface chemistry, and 13 nm and 50 nm nanoparticles were found to be exclusively carriers. After quantifying TEM images of nanoparticle–protein complexes, we can see that, though MUB-functionalized nanoparticles are cargo below 10 nm, MUA- and PEG-functionalized nanoparticles act as a carrier at 9 nm (Fig. 5B). These data suggest that, regardless of surface chemistries, ultrasmall nanoparticles act as cargo in nanoparticle–protein complexes. Nanoparticles near 10 nm in diameter can act as either cargo or as the carrier in nanoparticle–protein complexes depending on the surface chemistry of the particle. Therefore, researchers should be careful in considering the surface chemistry in their designs of sub-10 nm nanosystems to either take advantage of or avoid the propensity of their designs to act as cargo.

2.4. How does protein size mediate whether nanoparticles act as cargo or carrier?

So far, we have shown that below 10 nm, the gold nanoparticle's physicochemical properties do not appear to impact the overall structure of the nanoparticle–protein complex and can, therefore, be considered a cargo. Next, we wanted to confirm that the protein is indeed a carrier. The carrier's properties should dictate how the entire complex behaves both in transportation and interactions with physiological systems. To investigate whether the protein's properties affect the transportation of the nanoparticle–protein complex, we incubated 4 nm-CIT particles with proteins of various sizes. The 4 nm-CIT particles were incubated with proteins of similar isoelectric point but different molecular weights: insulin (pI = 5.3, 6 kDa) and transferrin (pI = 5.9, 80 kDa). Protein adsorption was confirmed using zeta potential measurements (see Fig. SI-4). After incubating nanoparticles with the proteins overnight at 37 °C, we performed agarose gel electrophoresis and compared the 4 nm-CIT particles with 50 nm-CIT particles that had

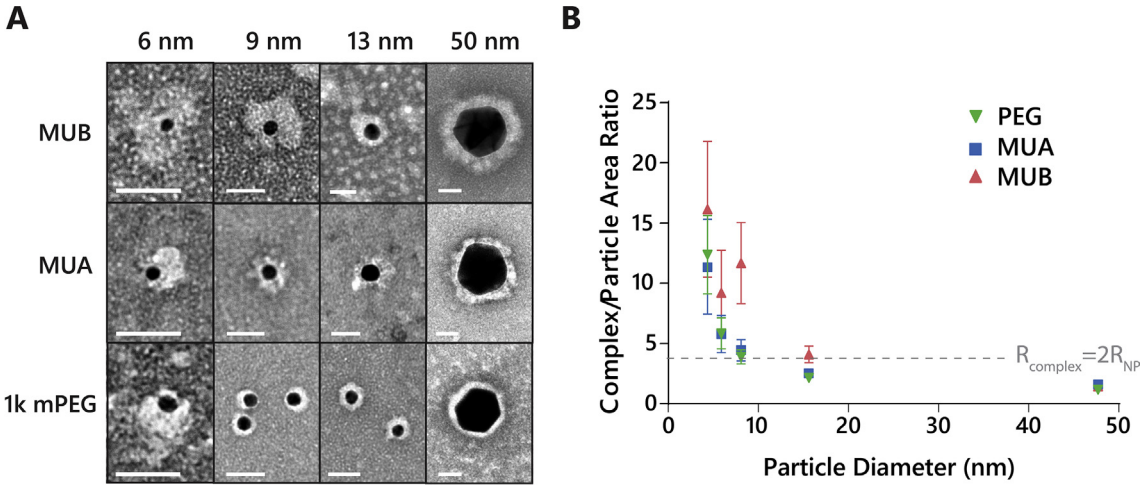

Fig. 5. A) Negative-stained TEM images of gold nanoparticles of various sizes and surface chemistries incubated with human serum. B) Image analysis of TEM images such as those in (A). The two-dimensional area was calculated from complex and nanoparticle diameters. The dotted line represents the point at which $R_{complex} = 2R_{particle}$. Scale bars represent 25 nm. Error bars represent the standard deviation of at least 200 measurements. (For interpretation of the references to colour in this figure legend, the reader is referred to the web version of this article.)

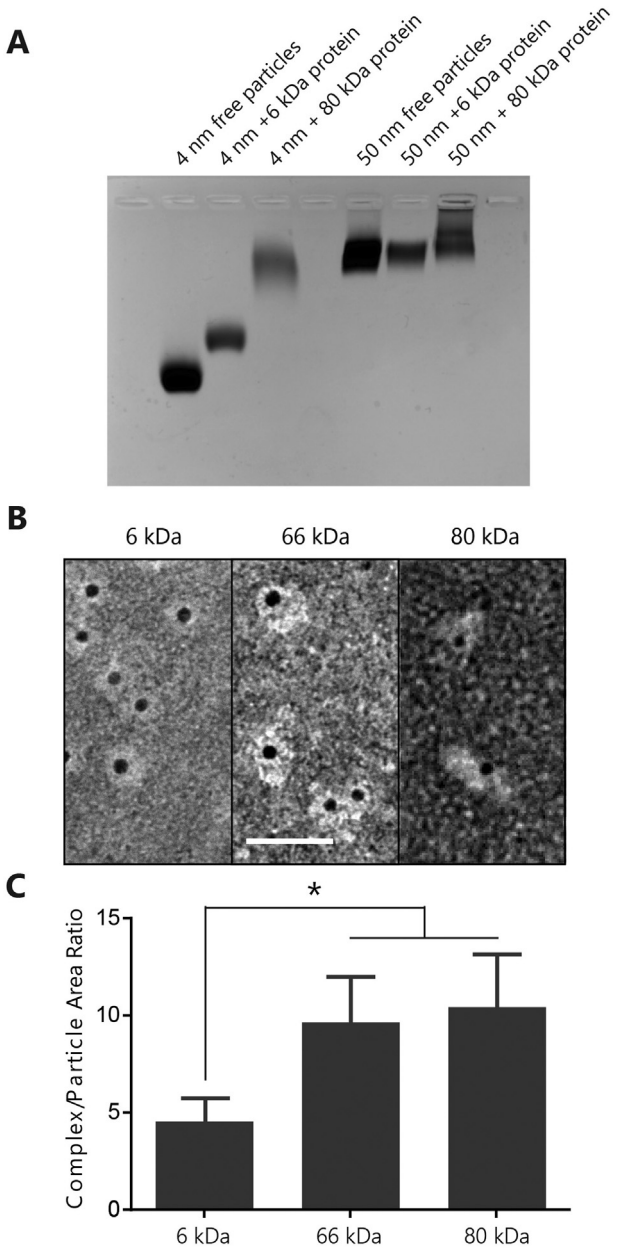

Fig. 6. Both 4 nm-CIT and 50 nm-CIT particles were incubated with insulin (6 kDa), BSA (66 kDa) or transferrin (80 kDa). A) Agarose gel electrophoresis of protein-incubated nanoparticles *versus* non-protein-coated nanoparticles. B) 4 nm-CIT particles were incubated with the indicated proteins, purified and imaged with TEM following negative staining with 1% uranyl acetate. C) Image analysis of TEM images of $n > 200$ complexes. Error bars indicate the standard deviation. All scale bars represent 25 nm. Asterisk indicates significant difference ($p < 0.001$).

undergone the same treatment. We found a striking difference between the migration distance of 4 nm-CIT particles incubated with different proteins (Fig. 6A). As would be expected for cargo, the nanoparticles migrated more when they were incubated with smaller proteins and less when they were incubated with larger proteins. In contrast, 50 nm-CIT particles travelled nearly identical distances regardless of the protein adsorbed. This indicates that the size of the 50 nm-CIT nanoparticle–protein complex is dominated by the nanoparticle physical properties and the proteins are the cargo in these complexes. To further probe the role of proteins as carriers, we performed TEM on 4 nm-CIT particles incubated with 6 kDa, 66 kDa (BSA) and 80 kDa proteins under negative stain conditions. We observed a qualitative difference in the types of complexes formed depending on the protein involved (Fig. 6B). We found that 4 nm-CIT particles incubated with 6 kDa proteins have a corona-like protein layer centred around the nanoparticle, whereas those incubated with the 66 and 80 kDa proteins formed complexes similar to those we saw with human serum above. The mean size of the complexes was significantly larger for both 66 kDa ($p < .001$) and 80 kDa ($p < .001$) than for the 6 kDa proteins, indicating that the size of the protein involved determines the size of the nanoparticle–protein complex (Fig. 6C). Our results demonstrate that provided the proteins are larger than ultrasmall nanoparticles, they will act as the carrier in nanoparticle–protein complexes. Since the most abundant proteins in human blood are albumins, globulin and fibrinogen, all of which are larger than ultrasmall nanoparticles, we estimate that a large majority of ultrasmall nanoparticles are cargo on protein carriers when administered *in vivo*. This study only investigated the effect of protein molecular weight on the structure of nanoparticle–protein complexes, but proteins have other physicochemical properties, such as deformability [13], that may affect their interactions with nanoparticles and should be investigated in future studies.

2.5. The biological impact of nanoparticles behaving as cargo

Having determined that the protein size determines the overall size of the ultrasmall nanoparticle–protein complex, we investigated a biological impact of a protein being a carrier rather than a cargo. We therefore decided to test the binding of proteins to their receptor target after the formation of nanoparticle–protein complexes with ultrasmall nanoparticle cargo. Trastuzumab was used as a model protein because it is an FDA-approved formulation used to target the HER2 receptor overexpressed by breast and ovarian cancers [14] and is also a large protein (148 kDa) well suited to the formation of complexes with ultrasmall nanoparticle cargo. Alexa-Fluor 750 (AF750) NHS ester was conjugated to the lysine residues on trastuzumab [15]. We incubated 4 nm-CIT and 50 nm-CIT nanoparticles with trastuzumab and determined a mean of 0.38 ± 0.03 proteins per nanoparticle for the 4 nm-CIT particles and 48 ± 2 proteins per nanoparticle for the 50 nm-CIT particles. We note that with each trastuzumab protein carrying approximately three 4 nm-CIT nanoparticles, the protein is clearly acting as a carrier. In this experiment, we incubated SKOV-3 ovarian cancer cells, a cell line that is known to express the HER2 receptor, with varying concentrations of trastuzumab-AF750 in its native form or adsorbed to 4 nm-CIT (nanoparticle cargo) or 50 nm-CIT (nanoparticle carrier), normalizing to the number of trastuzumab molecules added per cell (Fig. 7A). Both nanoparticle conditions were judged to be stable under experimental conditions (see Fig. SI-5). Labelled proteins or proteins adsorbed to nanoparticles were added to fixed SKOV-3 cells to allow for receptor-ligand interactions without the uptake and receptor recycling, and then binding was quantified using flow cytometry.

We hypothesized that a nanoparticle that functions as a cargo would act similarly to the native protein in its ability bind the HER2 receptor, while a nanoparticle that functions as a carrier would not, because they can bind to multiple receptors simultaneously. When a nanoparticle serves as a cargo, the binding properties of the protein would dominate, and when the nanoparticle serves as a carrier, the nanoparticle would affect the binding to the target. Using flow cytometry, we quantified the mean fluorescence intensity (MFI) per cell at different concentrations of trastuzumab. Native trastuzumab and trastuzumab adsorbed to nanoparticle cargo showed similar increases in fluorescence as we increased the concentration of trastuzumab (Fig. 7B). This increase in signal was not matched by trastuzumab absorbed to a 50 nm-CIT nanoparticle carrier, as this condition resulted in a much greater increase in MFI and reached a saturation point in the concentration range tested, whereas the other two conditions did not saturate. We would expect a greater increase in receptor binding for 50 nm-CIT particles with a trastuzumab corona due to the increased number of interactions that can occur from having a greater number of ligands on the particle and therefore greater

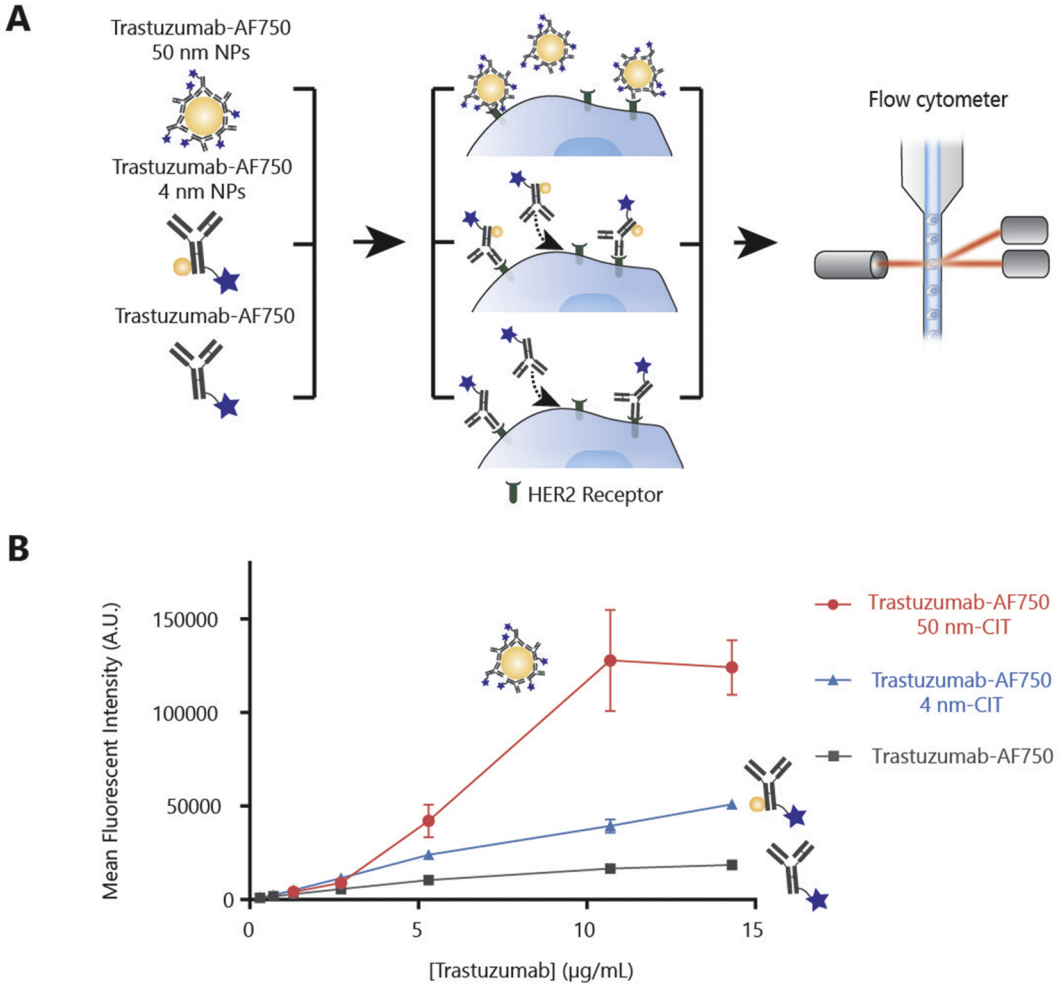

Fig. 7. A) Schematic of experimental design. Fixed SKOV-3 cells were incubated with various concentrations of AF750-labelled trastuzumab, either adsorbed to 50 nm-CIT or 4 nm-CIT nanoparticles or added independently. The cells were analyzed by flow cytometry to determine their mean fluorescent intensity. Figure is not drawn to scale. B) Mean fluorescent intensity of SKOV-3 cells incubated with AF750-labelled trastuzumab as cargo, carrier or without the presence of nanoparticles, as measured by flow cytometry. Error bars represent the standard deviation of at least 200 measurements.

avidity for the cell. Furthermore, since one nanoparticle can carry so many fluorophore-labelled proteins, one receptor–ligand interaction of a nanoparticle-bound trastuzumab can immobilize the nanoparticle carrier and result in a large fluorescent signal from all attached fluorophore-labelled proteins. This advantage, conferred on treatment or diagnostic moieties by the nanoparticle carrier, is frequently exploited by researchers. The fact that 4 nm-CIT cargo adsorbed to trastuzumab interacted with the receptor in a similar fashion to the native protein indicates that nanoparticles that act as cargo have little effect on protein binding function. This experiment not only demonstrated the different biological impacts of cargo and carrier nanoparticles, but suggests that sub-10 nm nanoparticles could be used in cases where protein function is best kept unhindered.

3. Conclusion

Here we have provided evidence that in nanoparticle–protein complexes formed with nanoparticles in the size realm of proteins (1 to 10 nm), the nanoparticles and proteins switch roles so that the protein becomes the carrier and the nanoparticle becomes the cargo. In these complexes, the nanoparticle physicochemical properties no longer have a large impact on the physicochemical properties of the complex, and the properties of the protein determine the biological interactions of the complex. Below the size at which nanoparticles go from carrier to cargo, the complexes formed with proteins may be better understood by studying complexes formed between proteins and particulate cargo than by studying the protein coronae formed by larger nanoparticles. The fact that the nanoparticles can act as cargo suggests that we may start to re-design our drug delivery platforms to take advantage of the physiological fate of the adsorbed proteins in the nanoparticle–protein complexes, similar to how some small molecule drugs take advantage of protein adsorption. As an example, aldoxorubicin is a conjugate of doxorubicin with a maleimide linker that binds as cargo to the free thiol on endogenous serum albumin when administered intravenously [16]. Having the drug as cargo on a protein carrier allows it to take advantage of the biodistribution of albumin without sacrificing the potency of the chemotherapeutic [17]. Future studies should focus on evaluating nanomaterials of different chemical compositions and surface chemistries, as the transition size point from the nanoparticle acting as carrier to cargo may vary from our reported value for gold nanoparticles. The results of these findings will diversify and enhance our design capability of nanoparticles for drug delivery and imaging applications.

4. Materials and methods

4.1. Materials

Gold (III) chloride ($HAuCl_4$), sodium citrate tribasic, tannic acid, potassium carbonate, Bis(*p*-sulfonatophenyl)phenylphosphine

dihydrate dipotassium salt (BSPP), magnesium chloride ($MgCl_2$), (11-mercaptoundecyl)-*N*,*N*,*N*-trimethylammonium bromide (MUB), 11-mercaptoundecanoic acid (MUA), fetal bovine serum (FBS), tetramethylammonium hydroxide (TMAH), human holo-transferrin, human recombinant insulin, bovine serum albumin (BSA), trichloroacetic acid (TCA), and formaldehyde were purchased from MilliporeSigma (Burlington, MA, USA). Tween-20, dithiothreitol (DTT) and phosphate buffered saline (PBS) were purchased from BioShop Canada Inc. (Burlington, ON, Canada). Dulbecco's modified Eagle's medium (DMEM), and Trypsin-EDTA (0.25%), Hanks' Balanced Salt Solution (HBSS), paraformaldehyde, and micro BCA kits were purchased from Thermo Fisher Scientific (Waltham, MA, USA). Thiolated methoxypolyethylene glycol (PEG, MW = 1 kDa) was purchased from Laysan BIO (Arab, AL, USA). Deoxycholic acid was purchased from Fluka – Honeywell Research Chemicals. Hydrochloric acid (HCl) and nitric acid were purchased from Caledon Laboratories (Georgetown, ON, Canada). NAP-5 columns were purchased from GE Healthcare Life Sciences (Marlborough, MA, USA). NuPAGE LDS sample buffer (4×) and AlexaFluor 750-NHS ester were purchased from Invitrogen (Carlsbad, CA, USA). Tris-Borate-EDTA (TBE) solution was purchased from Bio Basic (Markham, ON, Canada). DAPI stain and trastuzumab were purchased from Roche (Basel, Switzerland).

4.2. Gold nanoparticle synthesis and characterization

Gold nanoparticles were synthesized according to previous works [18]. In brief, 13 nm gold nanoparticles were synthesized by first adding 1.0 mL (1.0%*w/v*) of $HAuCl_4$ to deionized, distilled water (98 mL) in a 250 mL Erlenmeyer flask. The solution was brought to a boil on a stir plate set to 350 °C. Then, 1.0 mL of sodium citrate tribasic (3.0%w/v) was injected swiftly into the boiling solution under vigorous stirring. The reaction was allowed to proceed for 10 min, followed by cooling on ice. Obtained nanoparticles were stored at 4 °C prior to use.

To synthesize 3, 6 and 9 nm nanoparticles, 1.0 mL of $HAuCl_4$ (1.0% w/v) was added to 80 mL of deionized, distilled water in a 250 mL Erlenmeyer flask and brought to 60 °C on a stir plate. A reducing solution containing sodium citrate tribasic, tannic acid, and potassium carbonate was prepared according to the following table and warmed to 60 °C in a water bath for 50 min:

Nanoparticle size (nm)	**3 nm**	**6 nm**	**9 nm**
1.0%w/v Sodium citrate tribasic (mL)	6.0	6.0	6.0
1.0%w/v Tannic acid (mL)	7.5	0.8	0.2
3.46 mg/mL Potassium carbonate (mL)	7.5	–	–
Nanopure™ water (mL)	9.0	24	24

Under vigorous stirring, 20 mL of the reducing solution was swiftly injected into the Erlenmeyer flask and the reaction was kept at 60 °C for 30 min and then at 90 °C for 10 min. After cooling on ice, 1.0 mL of 80 mg/mL BSPP was added to the nanoparticle solutions and stirred overnight to improve particle stability. The obtained nanoparticles were washed three times by 30 min centrifugation using 0.01% sodium citrate aqueous solution containing 0.01% Tween 20. The centrifugation speed was 120,000 *g* for 3 nm, 80,000 g for 6 nm particles, and 25,000 g for 9 nm particles. The purified particles were stored at 4 °C prior to use.

50 nm gold nanoparticles were synthesized *via* seed-mediated growth, as described in previous works [12]. Briefly, 2.43 mL 15 nm gold nanoparticle seeds were added to 0.975 mL of each of hydroquinone, sodium citrate tribasic and $HAuCl_4$ in 94.6 mL of water during vigorous stirring at 4 °C. The mixture stirred for 12 h before being washed by centrifugation at 1800 *g* for with 0.02% sodium citrate buffer.

Synthesized nanoparticles were observed by TEM. 5 µl of nanoparticle solution (*ca.* 1–10 nM) was dropped on TEM grids, left for 3 min, and then blotted. The prepared samples were observed by TEM at 200 kV (Techni 20, FEI, Hillsboro, OR, USA). The diameter of nanoparticles was analyzed from the obtained TEM images by using ImageJ software. Nanoparticles were also characterized by dynamic light scattering (DLS) (Zetasizer Nano-ZS; Malvern Instruments Ltd., Worcestershire, UK), and ultraviolet-visible (UV–vis) spectroscopy (UV-1601PC; Shimadzu, Kyoto, Japan). Nanoparticle concentration was determined by UV–vis absorbance *via* the Beer–Lambert law, assuming that the extinction coefficient ε for gold nanoparticles can be described as a function of particle diameter D as follows:

$$\varepsilon = 10^{\left(1.0643 \ln\left(\frac{3}{2}\pi \cdot D^3\right)\right)+4.0935} \quad (4)$$

4.3. Gold nanoparticle functionalization

Gold nanoparticles were functionalized with MUA by adding a total nanoparticle surface area of 40 cm^2 to 100 µL of 3 mM MUA in ethanol. After mixing with a pipette, the mixture was incubated in a water bath at 60 °C for one hour. 10 µL of 300 mM TMAH was added, and the suspension was centrifuged and resuspended in 3 mM TMAH. The nanoparticles were centrifuged a second time and resuspended in 1 mM NaOH for storage at 4 °C.

For functionalization with MUB, 40 cm^2 of nanoparticles were added to 100 µL of 30 mM MUB in ethanol. After quick mixing an incubation at 60 °C for one hour, nanoparticles were washed twice, resuspending both times in water.

Nanoparticles were PEGylated by mixing nanoparticles with 1 k mPEG at a ratio of 5 PEG/nm^2. The solution was vortexed and left to incubate overnight at room temperature or for one hour at 60 °C. Nanoparticles were then washed twice, resuspending in water.

4.4. Nanoparticle–protein incubation and purification

Human serum was filtered through a 0.22 µm cellulose filter to remove aggregates. 90 nm^2 total nanoparticle surface area in 200 µL of water was added to 200 µL human serum, and the mixture was incubated for one hour at 37 °C. For experiments involving specific proteins, proteins were dissolved in 200 µL of PBS at a concentration of 600 µM.

Following incubation, nanoparticles were centrifuged three times, resuspending in 0.5× PBS each time. 4 nm nanoparticles were not simply centrifuged because we were concern that the high-speed centrifugation would also pellet large proteins. Instead, we performed sucrose gradient purification with a 60% and a 40% sucrose layer. Samples were floated on top of the two sucrose layers and centrifuged at 180000 *g* for one hour to separate nanoparticle–protein complexes from free proteins based on density. Following centrifugation, the top protein layer was removed prior to recovering nanoparticle–protein complexes from the bottom of the centrifuge tube. Sucrose was then removed from nanoparticle–protein complexes by filtration through a 3 kDa amicon spin filter. After five washes with 0.5× PBS, the procedure was repeated for a second wash. Zeta potential measurements (see Fig. SI-6) confirmed the presence of adsorbed proteins.

4.5. Agarose gel electrophoresis

After incubation and without purification, nanoparticle–protein complexes were mixed with glycol and loaded into the wells of a 1% agarose gel made with 0.05× TBE in a tank filled with 0.05× TBE. Samples were run at 100 V. Gels were imaged on a Gel Doc™ EZ Gel Documentation System (Bio-Rad Laboratories, Hercules, CA, USA).

4.6. Negative staining of nanoparticle–protein complexes

5 µL of sample was added to plasma treated grids and incubated for

three minutes before being blotted. Water was then added to the grid (2 μL) and then blotted after one minute. Uranyl acetate (1%, 2 μL) was then added to the grids for one minute before being blotted. To ensure that protein corona was being stained as opposed to the PEG layer on PEGylated nanoparticles, we also stained non-incubated PEGylated nanoparticles and compared the size of the highlighted area to that of incubated PEGylated nanoparticles (see Fig. SI-7).

4.7. Image analysis

TEM images of nanoparticle–protein complexes were analyzed using the Fiji image processing program. Particle diameters were determined using the *analyze particles* function, while complex diameters were measured by drawing a straight line vertically through the centre of the nanoparticle from one end of the negative-stained area to the other (see Fig. SI-8). Where complexes were clearly aggregated, partially outside of the image frame, or boundaries of staining were not clearly defined, the measurements were not taken.

4.8. Quantification of adsorbed proteins

Proteins were first stripped from nanoparticles as follows: To 20 μL of nanoparticles, 8 μL of NuPAGE LDS sample buffer (4 ×) and 4 μL of 500 mM DTT were added. The mixture was vortexed briefly and incubated at 70 °C for one hour. It was then centrifuged for 15 min at room temperature, and 18,000 g and the supernatant was collected. 950 μL of 10% TCA in acetone was added to the sample, and it was left overnight at −80 °C. The solution was centrifuged again for 15 min at 4 °C and 18,000 g and the supernatant discarded. The pellet was re-suspended in 500 μL 0.03% deoxycholic acid in water, vortexed briefly and left on ice for one hour to precipitate protein. Samples were centrifuged again at 18000 *g*, supernatant was removed, and pellet was washed in 950 μL of cold acetone. The mixture was left at −80 °C for one hour to re-precipitate the protein. The proteins were again centrifuged at 18000 *g*, the supernatant was discarded, and the pellet was left to air dry for one hour to remove acetone. Proteins were then re-suspended in 50 μL PBS and heated to 70 °C for one hour to solubilize proteins. Standards for the ensuing BCA assay were processed using the same procedure as samples. 200 μL BCA working reagent (as described in the protocol for the micro BCA assay) was then added to each sample or standard and the samples were incubated at 60 °C for 15 min to develop colour. Finally, samples and standards were transferred to a 96-well plate and absorbance at 562 nm was measured using a Sunrise microplate reader (Tecan Life Sciences, Männedorf, Switzerland).

4.9. Trastuzumab modification

Trastuzumab proteins were modified with Alexa-Fluor 750 (AF750) prior to use. To remove trace amounts of sodium azide present in lyophilized trastuzumab, trastuzumab was dialyzed overnight against 0.1 M sodium bicarbonate buffer (pH 8.6) in 3.5 kDa MW dialysis filters. Concentration was determined by measuring absorbance at 280 nm and a molar extinction coefficient of $\varepsilon_{280} = 2.18 \times 10^5\,M^{-1}\,cm^{-1}$. A 2 times molar excess of NHS-AF750 was added to the trastuzumab solution and the mixture was incubated in the dark, overnight at 4 °C. The Trastuzumab-AF750 was purified using a GE Healthcare size-exclusion column according to manufacturer's protocols. Labelling efficiency and protein concentration were determined from absorbance measurements of the protein and fluorophore complex at 280 nm and 750 nm. Aliquots of Trastuzumab-AF750 were stored in the dark at −80 °C and thawed just prior to use.

4.10. Adsorption of trastuzumab and quantification

4 and 50 nm citrate-coated nanoparticles were mixed with Trastuzumab-AF750 at molar ratios of 2:1 and 200:1 respectively in 0.1 × PBS. Mixtures were incubated at 37 °C for one hour then washed by centrifugation twice into 0.1 X PBS. To quantify the number of proteins per nanoparticle, a depletion assay was performed in triplicate by collecting supernatant after the washes (see Fig. SI-9). The supernatant's fluorescent intensity at 775 nm was measured after excitation at 730 nm by a Horiba Fluoromax-3 (Kyoto, Japan). Fluorescence was compared to a standard curve of trastuzumab-AF750, and the number of proteins on the particles was determined from the concentration remaining in solution.

4.11. Cell culture

SKOV-3 ovarian cancer cells were grown in DMEM supplemented with 10% FBS and 1% penicillin/streptomycin. Cells were maintained in a humidified incubator at 37 °C with 5% CO_2.

4.12. Cell binding

SKOV-3 cells were grown to 80% to 90% confluency in T75 cell culture flasks (NEST Biotechnology Co., Wuxi, China). They were harvested using 0.25% trypsin-EDTA and split into Eppendorf tubes with 1×10^6 cells per tube. Cells were washed twice in PBS (300 g, 3 min) and then fixed in 1.6% paraformaldehyde in HBSS for 30 min on ice. They were then washed twice in PBS and cooled on ice. The indicated concentrations of AF750-labelled trastuzumab or the same protein pre-adsorbed to gold nanoparticles were added to the cells and mixed with a pipette, and the cells were incubated on ice for two hours (total volume 150 μL). Following incubation, cells were centrifuged three times (100 *g*, 10 min) into 900 μL of HBSS supplemented with 0.5% BSA and 10 mM EDTA and stored in the dark at 4 °C for a maximum of 2 days.

4.13. Flow cytometry

Events were acquired with a BD LSR Fortessa X-20 (BD BioSciences). Gating was based on fluorescence-minus-one (FMO) control. Data were analyzed using FlowJo 10.0.7 (TreeStar Inc.).

Acknowledgements

The project was supported by the Canadian Cancer Society (705185-1), Canadian Institutes of Health Research (CIHR) (FDN159932, MOP-130143) and Natural Sciences and Engineering Research Council of Canada (NSERC) (2015-0639), and Canadian Research Chairs Program (950-223824). D. G. thanks NSERC for the Alexander Graham Bell Canada Graduate Scholarship and the department of chemistry for the Leslie Gladstone Cook Memorial Fellowship. B.O. thanks the Vanier Canada Graduate Scholarship, CIHR and the McLaughlin Centre for MD/PhD studentships, and the Donnelly Centre for graduate fellowships. J. Z. thanks the Ontario Ministry of Training, Colleges and Universities and the University of Toronto for the Queen Elizabeth II Graduate Scholarship in Science and Technology. J. L. Y. W. thanks the Barbara & Frank Milligan Graduate Fellowship. S. O. acknowledges the Japan Society for the Promotion of Science for a research fellowship (PD, No. 5621) and KAKENHI (16 K14468).

Declarations of interest

None.

Appendix A. Supplementary data

Supplementary data to this article can be found online at https://doi.org/10.1016/j.jconrel.2019.04.023.

References

[1] B. Pelaz, et al., ACS Nano 50 (2017) 2313–2381.
[2] T. Cedervall, I. Lynch, S. Lindman, T. Berggård, E. Thulin, H. Nilsson, K.A. Dawson, S. Linse, Proceedings of the National Academy of Sciences, vol. 104, (2007), pp. 2050–2055 M. P. Monopoli, C. Åberg, A. Salvati, K. A. Dawson, *Nat. Nanotechnol.* 2012, *7*, 779; P. C. Ke, S. Lin, W. J. Parak, T. P. Davis, F. Caruso, *ACS Nano* vol. 11, 2017, 11773-11776.
[3] S. Lara, F. Alnasser, E. Polo, D. Garry, M.C. Lo Giudice, D.R. Hristov, L. Rocks, A. Salvati, Y. Yan, K.A. Dawson, ACS Nano 11 (2017) 1884–1893.
[4] N. Bertrand, P. Grenier, M. Mahmoudi, E.M. Lima, E.A. Appel, F. Dormont, J.-M. Lim, R. Karnik, R. Langer, O.C. Farokhzad, Nat. Commun. 8 (2017) 777.
[5] C.D. Walkey, J.B. Olsen, H. Guo, A. Emili, W.C. Chan, J. Am. Chem. Soc. 134 (2012) 2139–2147.
[6] A.E. Nel, L. Mädler, D. Velegol, T. Xia, E.M. Hoek, P. Somasundaran, F. Klaessig, V. Castranova, M. Thompson, Nat. Mater. 8 (2009) 543 (D. Walczyk, F. B. Bombelli, M. P. Monopoli, I. Lynch, K. A. Dawson, *J. Am. Chem. Soc.* vol. 132, 2010, 5761-5768).
[7] C.D. Walkey, W.C. Chan, Chem. Soc. Rev. 41 (2012) 2780–2799 (A. Albanese, C. D. Walkey, J. B. Olsen, H. Guo, A. Emili, W. C. Chan, *ACS Nano* vol. 9, 2014, 5515-5526).
[8] C.D. Walkey, J.B. Olsen, F. Song, R. Liu, H. Guo, D.W.H. Olsen, Y. Cohen, A. Emili, W.C. Chan, ACS Nano 8 (2014) 2439–2455.
[9] S. Lindman, I. Lynch, E. Thulin, H. Nilsson, K.A. Dawson, S. Linse, Nano Lett. 7 (2007) 914–920.
[10] M.P. Monopoli, D. Walczyk, A. Campbell, G. Elia, I. Lynch, F. Baldelli Bombelli, K.A. Dawson, J. Am. Chem. Soc. 133 (2011) 2525–2534.
[11] H.P. Erickson, Biological Procedures Online, vol. 11, (2009), p. 32.
[12] S.D. Perrault, W.C. Chan, J. Am. Chem. Soc. 131 (2009) 17042–17043.
[13] J.M. Dennison, J.M. Zupancic, W. Lin, J.H. Dwyer, C.J. Murphy, Langmuir, (2017).
[14] M. Colombo, L. Fiandra, G. Alessio, S. Mazzucchelli, M. Nebuloni, C. De Palma, K. Kantner, B. Pelaz, R. Rotem, F. Corsi, Nat. Commun. 7 (2016) 13818 (A. M. Scott, J. D. Wolchok, L. J. Old, *Nat. Rev. Cancer* vol. 12, 2012, *12*, 278).
[15] Q. Dai, S. Wilhelm, D. Ding, A.M. Syed, S. Sindhwani, Y. Zhang, Y.Y. Chen, P. MacMillan, W.C. Chan, ACS Nano 12 (2018) 8423–8435.
[16] F. Kratz, R. Müller-Driver, I. Hofmann, J. Drevs, C. Unger, J. Med. Chem. 43 (2000) 1253–1256.
[17] F. Kratz, J. Control. Release vol. 132, (2008) 171–183 (C. Unger, B. Häring, M. Medinger, J. Drevs, S. Steinbild, F. Kratz, K. Mross, *Clin. Cancer Research* vol. 13, 2007,4858-4866).
[18] L.Y. Chou, K. Zagorovsky, W.C. Chan, Nat. Nanotechnol. 9 (2014) 148–155.